Soft Matter

www.rsc.org/softmatter

Volume 9 | Number 23 | 21 June 2013 | Pages 5503–5658

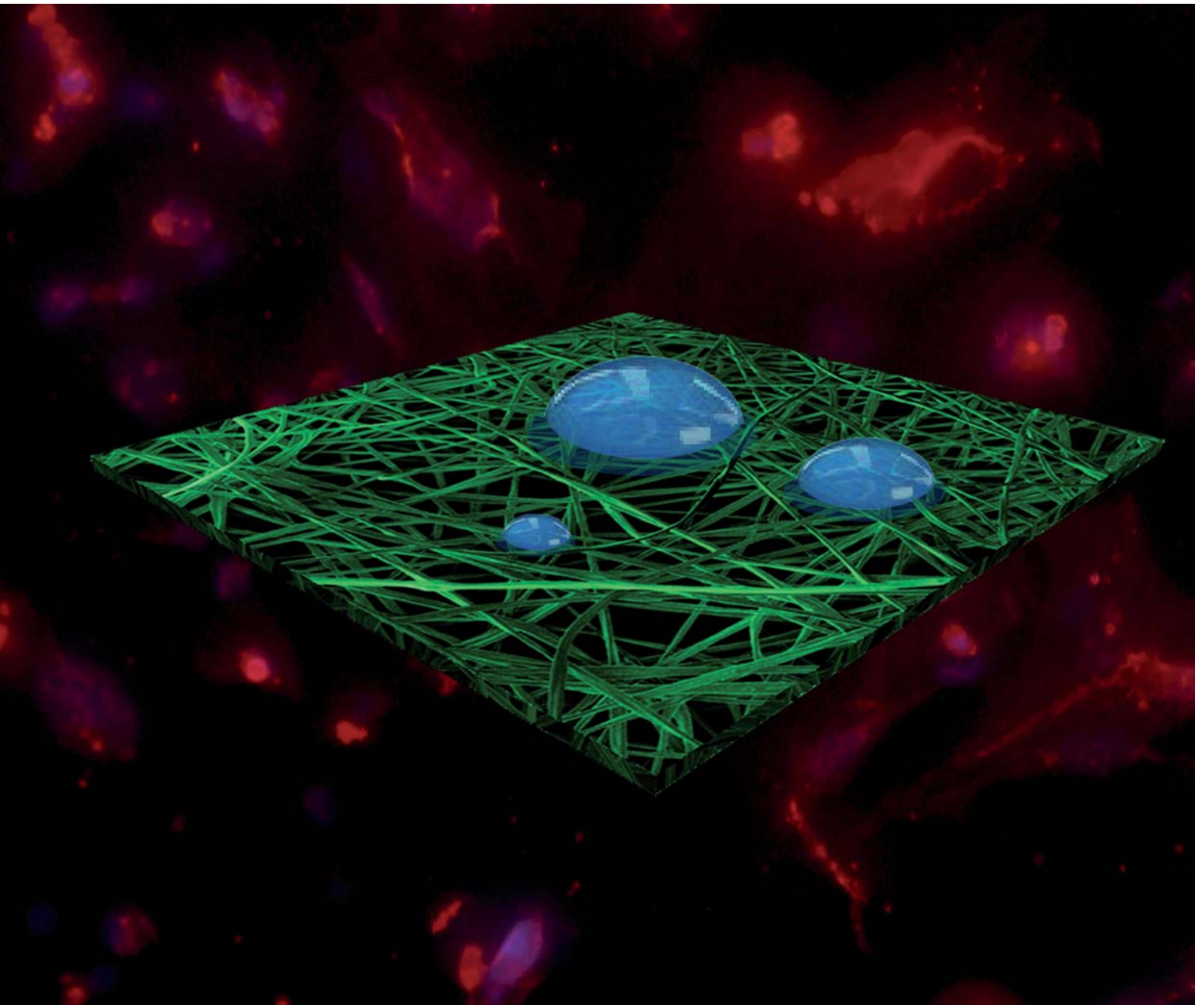

ISSN 1744-683X

RSC Publishing

PAPER

Maria Moffa, Dario Pisignano *et al*.

Microvascular endothelial cell spreading and proliferation on nanofibrous scaffolds by polymer blends with enhanced wettability

1744-683X(2013)9:23;1-5

Soft Matter

RSC Publishing

PAPER

Microvascular endothelial cell spreading and proliferation on nanofibrous scaffolds by polymer blends with enhanced wettability

Cite this: *Soft Matter*, 2013, **9**, 5529

Maria Moffa,*[ab] Alessandro Polini,†[c] Anna Giovanna Sciancalepore,[a] Luana Persano,[ac] Elisa Mele,‡[a] Laura Gioia Passione,[ab] Giovanni Potente[cd] and Dario Pisignano*[abc]

The objective of this study is elucidating the mechanisms by which the wettability of nanofibrous electrospun mats varies in polymer blends, and highlighting how this can play a pivotal role in enhancing the viability of cultured microvascular endothelial cells (EC). A functional microvascular network is essential for supplying bioengineered tissues with oxygen and nutrients while removing metabolic wastes. An *in vitro* pre-vascularization strategy consists of seeding EC on scaffolds, which in turn promotes cells infiltration, adhesion and functionality. We use electrospun poly-L-lactic acid (PLLA) and gelatin (Gel) as prototype materials for realizing nanofibrous scaffolds as bioartificial architectures to improve the proliferation and the functionality of human microvascular ECs (HMEC-1). HMEC-1 seeded on electrospun scaffolds adhere, remain viable, proliferate and positively express the endothelial cell marker CD31 particularly on blend PLLA/Gel fibers, which exhibit wettability enhanced with respect to both the constituent polymers, and are therefore especially promising constructs for promoting the formation of functional endothelial tissue. The wettability characteristics of the blend polymer fibrous scaffolds are modeled and discussed. These results can be valuable for the future design of pre-vascularized scaffolds with enhanced wettability properties for functional tissue engineered implants, with ECs able to form in perspective an effectively functioning vasculature upon implantation.

Received 31st January 2013
Accepted 21st March 2013

DOI: 10.1039/c3sm50328c

www.rsc.org/softmatter

Introduction

The multidisciplinary field of tissue engineering has the ultimate aim of repairing and/or replacing damaged tissues or organs by means of a properly designed combination of functional cells and scaffolding biomaterials. The latter have to support cell anchorage and growth, and to faithfully replicate the biological and mechanical properties of endogenous extracellular matrix (ECM).[1,2] A few critical issues are to be taken into careful consideration for the achievement of successful regeneration events, including the vascularization of bioengineered constructs and the physical properties of the scaffold, in order to mimic the *in vivo* microenvironment and trigger the specific tissue morphogenesis.[3,4] In addition, an artificial implant is fully functional only if it is connected to the host vascular system, which is vital to supply nutrients and oxygen, allow clearance of metabolic waste and maintain tissue homeostasis.[5] Vascularization currently remains one of the major challenges for the therapeutic success of engineered bio-scaffolds. Since the spontaneous growth of the vascular system in a bioartificial tissue is a slow process, limited to tenths of micrometers per day, the viability of the construct can be prejudiced *in vivo* for different weeks after implantation.[5] Consequently, regenerative medicine has been successfully applied especially to thin or avascular tissues, such as cartilage and skin, for which the postimplantation neovascularization from the host is adequate to provide oxygen and nutrients to the implant.[6]

A strategy recently proposed for the vascularization of big tissues and organs is the *in vitro* pre-vascularization of the constructs.[5,7] This procedure is based on the principle that, under favorable culture conditions and physical microenvironments, endothelial cells (ECs) spontaneously organize into capillary-like structures, which anastomose to the host vessels, supplying the construct with nutrients.[8] Pre-vascularization approaches have been studied for several engineered tissues,

[a]*Center for Biomolecular Nanotechnologies @UNILE, Istituto Italiano di Tecnologia, via Barsanti, I-73010 Arnesano, LE, Italy. E-mail: maria.moffa@iit.it; dario.pisignano@unisalento.it*

[b]*Dipartimento di Matematica e Fisica "Ennio De Giorgi", Università del Salento, via Arnesano, I-73100 Lecce, Italy*

[c]*National Nanotechnology Laboratory of Consiglio Nazionale delle Ricerche-Istituto Nanoscienze, via Arnesano, I-73100 Lecce, Italy*

[d]*Istituto Superiore di Formazione Interdisciplinare ISUFI, Università del Salento, via Arnesano, I-73100 Lecce, Italy*

† Present address: Lawrence Berkeley National Laboratory, Materials Sciences Division, 1 Cyclotron Road, 94720, Berkeley, CA, USA.

‡ Present address: Nanophysics, Istituto Italiano di Tecnologia (I.I.T.), *via* Morego 30, 16163 Genova, Italy.

including bone, kidney, skeletal and cardiac muscle,[5] speeding up the vascularization from weeks to days,[9] and enhancing the survival and the functionality of the scaffolds. To succeed in the pre-vascularization, the availability of appropriate biomaterials, in terms of surface morphology, stiffness and topography, is fundamental to support EC growth and proliferation, favoring cell–scaffold interactions and ultimately tissue formation.[2] To this aim, electrospinning (ES) has been proposed as an effective and low-cost technique to fabricate ultra-thin fibers (diameter down to below 1 μm depending on the polymer species and processing conditions), mimicking the ECM architecture,[10,11] and promoting growth and differentiation of various cell types, such as human mesenchymal stem cells,[12] ECs,[13] fibroblasts,[14] myoblasts,[15] and osteoblasts.[16] Moreover, ES provides a useful strategy to blend synthetic polymers with various biopolymers, which together show unique combinations of mechanical, durability and biocompatibility properties. For instance, ES allows to process elastin–poly(DL-lactide-*co*-glycolide) for vascular graft scaffolds,[17] collagen–poly(caprolactone) (PCL) for bioengineering of human skin,[18] chitosan–polyethylene oxide (PEO) for wound dressings and drug delivery,[19] and gelatin–PCL for nerve regeneration.[20]

Here we analyze the effect of blending polymers in order to realize nanofibrous scaffolds to promote the proliferation of human microvascular ECs (HMEC-1). This is one of the best characterized immortalized endothelial cell lines.[21] Importantly, the strategic interest in HMEC-1 for tissue engineering applications is because they retain many characteristics of endothelial cells, with the advantage of avoiding the isolation, purification and growth of primary cells.[22] Furthermore, these cells are particularly useful to understand the behavior of microvascular endothelial cells in several physiologic and pathophysiological processes.[22] Finally, with respect to other common ECs (extracted for instance from an umbilical vein), these cells offer a distinctive advantage in perspective, since they could be isolated from the same patient who will receive the scaffold.[23] In particular, we focus on the wettability properties of polymer blends, which are enhanced with respect to both the individual constituent polymers and are here demonstrated to play an important role in favoring the adhesion and viability of ECs. In fact, though generally recognized as a cofactor influencing cell adhesion on culture surfaces, the wetting behavior of blend nanofibrous scaffolds, its relation with the properties of the polymer components, and its influence on the adhesion and proliferation of microvascular cells have not been studied yet. The elucidation of these mechanisms can provide important indications for designing novel scaffold structures with tailored wettability and surface properties. Among interesting synthetic polymers, poly-L-lactic acid (PLLA) offers many advantages since it is a biocompatible and biodegradable polyester approved by the Food and Drug Administration (FDA), it is a low-cost material, it is easy to process, and it is especially suitable for tissue engineering due to its controllable and widely studied mechanical properties.[24–26] Unfortunately, the hydrophobic nature of PLLA hinders cell seeding[27] and makes nanofibrous scaffolds that are lacking in cell recognition signals. To avoid this drawback, different methods have been proposed, mainly based on functionalization by ECM molecules through physical coatings or chemical grafting.[28] In particular, a promising opportunity is provided by processing PLLA with natural biopolymers, such as gelatin (Gel).[29] Derived from collagen which is the major component of skin, bone, cartilage and connective tissues, and due to its high cytocompatibility, Gel is known to be a very advantageous biomaterial for scaffold design, though it is rarely used in mono-component nanofibrous scaffolds because of its poor mechanical properties and high water solubility.[30] Blends of Gel and PLLA allow instead to produce nanofibrous scaffolds with good cell adhesion and mechanical properties.[29,31] Gu *et al.*[31] have demonstrated the excellent biocompatibility of PLLA/Gel nanofibers (NFs) with human embryonic fibroblasts and their potential application in wound dressing. Kim *et al.* produced PLLA/Gel polymeric NFs as a bone cell supporting matrix.[29] Composite scaffolds of PLLA/collagen and apatite have been also investigated aiming at bone regeneration.[32] However, neither the underlying mechanisms determining the wettability properties of nanofibrous PLLA/Gel scaffolds nor to what extent human microvascular ECs adhere and are affected by the blend properties has been analyzed in depth. We here find that ECs remain viable, proliferate and positively express CD31 as an endothelial cell marker on the produced scaffolds, with higher proliferation observed for blend electrospun scaffolds with enhanced wettability. These results can be valuable for tissue engineering approaches aimed at designing and realizing pre-vascularized scaffolds and functional blood vessel networks with enhanced wettability properties.

Materials and methods

Materials

PLLA (molecular weight of 85–160 kg mol^{-1}), gelatin type B from bovine skin, EDC, NHS, 0.05% (w/v) trypsin, penicillin–streptomycine solution (105 units of penicillin per ml and 10 mg streptomycin per ml), hydrocortisone, L-glutamine, 4′,6-diamidino-2-phenylindole dihydrochloride (DAPI), phalloidin-FITC, Triton® X100, albumin from bovine serum (BSA), paraformaldehyde and organic solvents were purchased from Sigma-Aldrich (St. Louis, MO). Cr granulate is from Umicore Materials AG (Brussels, Belgium). HFIP is from Carlo Erba (Milan, Italy). Fetal bovine serum (FBS), medium 199 and phosphate buffered saline (PBS) are from Lonza (Milan, Italy). Cell-Titer 96 AQueous One Solution Cell Proliferation Assay (MTS) is from Promega (Milan, Italy). Mouse anti-CD31 is from Millipore (Milan, Italy). Alexa Fluor® 555 Goat Anti-Mouse IgG is from Invitrogen Inc. (Paisley, UK). Recombinant Human epidermal growth factor (EGF) is from PeproTech Inc. (Rocky Hill, NJ). HMEC-1 were established by Prof. E. W. Ades, Center for Disease Control (Atlanta, GA),[33] and kindly provided by Dr G. Turchi (Consiglio Nazionale delle Ricerche-IBF, Pisa, Italy).

Scaffold fabrication

For the ES process, solutions of PLLA, Gel and PLLA/Gel (1 : 1 in weight) using hexafluoroisopropanol (HFIP) as solvent and a

concentration (w/w) of 8.0%, 3.5%, and 4.0%, respectively, are prepared and stirred for 24 h. Further samples are realized for contact angle and morphology measurements, with a solution concentration (w/w) of 4.0% in HFIP and a PLLA : Gel relative weight of 100 : 0, 90 : 10, 70 : 30, 50 : 50, 30 : 70, and 0 : 100, respectively. Each solution is loaded in a plastic syringe with a 27 gauge stainless steel needle. A voltage of 7.5 kV is applied to the needle for spinning PLLA, and of 4.5 kV for Gel and PLLA/Gel, by a high voltage power supply (EL60R0.6-22, Glassman High Voltage, High Bridge, NJ). During ES, the injection flow rate is kept constant at 0.5 ml h^{-1} using a syringe pump (Harvard Apparatus, Holliston, MA). NFs are collected for 1 h on borosilicate glass coverslips with area from 1.7 to 19 cm^2, mounted on a grounded 10 × 10 cm^2 collector at a distance of 20 cm from the needle. The air relative humidity and temperature are about 40% and 20 °C, respectively. Most of the HFIP would evaporate during the ES process. In addition, all the samples are stored in a vacuum desiccator at room temperature for two days to remove HFIP residues. For crosslinking, Gel and PLLA/Gel scaffolds are immersed in EDC/NHS (50 mM/50 mM) ethanol solution for 24 h at 4 °C. Afterwards, the NFs are washed with distilled water three times, and sterilized in 70% ethanol for 1 h. Before cell culture, the nanofibrous substrates are prewet in PBS and treated by oxygen plasma with a tabletop system (Tucano, Gambetti Kenologia, Milano, Italy) at 30 W for 5 min to improve the wetting properties before sterilization and cell seeding. Reference PLLA, Gel, and PLLA/Gel films for contact angle measurements and morphological observation are spin-cast on borosilicate glass coverslips from the same electrospinning solution, at 5000 rpm for 50 s.

Scaffold characterization

The diameter and morphologies of electrospun samples are determined by scanning electron microscopy (SEM, Raith, Dortmund, Germany) after thermal deposition of 5 nm of Cr (PVD75, Kurt J. Lesker Co.), using an accelerating voltage of 5 kV and an aperture size of 20 μm. The average diameter of the fibers is calculated from the SEM micrographs by imaging software (WSxM, Nanotec Electronica, Madrid, Spain), analyzing a total number of at least 100 NFs for each sample category. The composition of the produced scaffolds is evaluated by Attenuated Total Reflection Fourier Transform-Infrared (FTIR) spectroscopy (Spectrum 100, Perkin Elmer, Waltham, MA) using a ZnSe 45-degree flat-plate (Perkin Elmer), in a range of 4000–500 cm^{-1} and with a resolution of 4 cm^{-1}. For degradation tests ($n = 5$ specimens), the scaffolds are placed in PBS (pH 7.2) and incubated at 37 °C for different periods of time, up to 30 days.[34] After each degradation period (1, 15 and 30 days), the NF substrates are washed in distilled water, dried in a vacuum desiccator at room temperature for 48 h, and finally weighed. The weight loss percentage of each specimen is calculated as:[34] weight loss (%) = $[(W_1 - W_2)/W_1] \times 100$, where W_1 and W_2 are the weight of the sample before and after the degradation test, respectively. Mechanical properties are determined using a dynamic mechanical analyzer (DMA Q800, TA Instruments, New Castle, DE). Each sample ($n = 10$ specimens) is cut into rectangular shapes (5 × 30 mm^2) before testing, and its thickness is measured using a digital micrometer (0.03–0.06 mm). The stress–strain curves are recorded with a ramp/rate of 1 N min^{-1} (up to 18 N), and elastic modulus, percentage elongation, and ultimate tensile strength are obtained. The morphological characterization of reference spin-coated films is carried out by tapping atomic force microscopy (AFM) in air, using a Nanoscope III controller with a Multimode head (Veeco) and integrated with an E-scanner. P-doped Si tips are used with an 8 nm nominal curvature radius and a resonant frequency of 190 kHz. Finally, the apparent contact angle of water (WCA) on the scaffolds is measured using an Optical Video Contact Angle System (CAM-200, KSV Instruments, Helsinki, Finland), gently delivering a drop (≈2 μL) of ultrapure water from a capillary tip onto the fiber surface ($n = 5$ specimens).

Cell culture

HMEC-1 cells are established from Human dermal Microvascular Endothelial Cells (HMEC) and immortalized by transfection with a pBR322-based plasmid containing the coding region for the simian virus 40 large T-antigen.[33] HMEC-1 are maintained in an M199 medium containing 10% FBS, 10 ng ml^{-1} EGF, 1 mg ml^{-1} hydrocortisone, 1% penicillin–streptomycine, and 2 mM L-glutamine. Cells are subcultured at least once a week, and maintained in a humidified atmosphere (5% CO_2 in air) at 37 °C.

Cell seeding and proliferation

Confluent cells in a flask are washed with PBS, removed with a trypsin–EDTA solution and seeded onto PLLA, Gel, and PLLA/Gel nanofibrous scaffolds, in 24-well plates, at a concentration of 3 × 10^4 cells per ml. For all the samples, the culture medium is replaced every 3 days. Cell viability on the nanofibrous substrates is evaluated after 2, 4, and 8 days by MTS assay. At each time point, MTS solution is added to the medium in all the wells. Cells are then incubated at 37 °C for 4 h and the absorbance is determined at 490 nm using a spectrophotometer (Spectrum 100, Perkin Elmer, Waltham, MA).

Cell morphology and phenotype study

Immunocytochemistry analysis is performed in order to assess HMEC-1 cell morphology and to verify that these cells retain an endothelial phenotype on the nanofibrous scaffolds. Cells are starved on PLLA, Gel and PLLA/Gel scaffolds placed in 24-well plates, at a concentration of 3 × 10^4 cells per ml for 8 days. To perform immunocytochemistry and three dimensional occupation analysis, samples are fixed in 4% paraformaldehyde for 30 min and washed 3 times with PBS for 5 min each. Cell membranes are permeabilized by incubation with 0.1% (v/v) Triton-X100 in PBS for 15 min, followed by incubation in 1% BSA (w/v) in PBS for 30 min to reduce nonspecific background staining. For morphological evaluations, samples are stained for 30 min with phalloidin-FITC (25 μg ml^{-1}). Then, they are washed with PBS and incubated with DAPI (6 μg ml^{-1}) for 15 min. To visualize the marker CD31, samples are incubated for 2 h in

mouse anti-CD31 (1 : 50), as a primary antibody, and then washed with PBS and incubated with the secondary antibodies anti mouse (Alexa Fluor 555 conjugated, 1 : 250) for 1 h. Nuclei are stained by using DAPI for 15 min. Finally, scaffolds are visualized using an epifluorescence microscope (Eclipse Ti, DAPI-FITC-TRITC filters, Nikon, Melville, NY) equipped with a Nikon DS-Ri1 camera. The HMEC-1 three dimensional occupation of sub-surface pores within the scaffolds is studied by confocal microscopy (Nikon). Serial z plane sampling is performed on DAPI stained HMEC-1 cells grown for 8 days on electrospun scaffolds, for a total z-scan distance of 80 μm at 1 μm per plane.

Statistical analyses

The NF diameter, contact angles, mechanical properties, degradation test and viability test results are expressed as (mean ± standard deviation). A one-way analysis of variance (ANOVA) with Tukey's post hoc test for multiple comparisons is used for statistical analysis and a P value >0.05 is considered statistically significant.

Results and discussion

Scaffold characterization and wettability properties

The morphology of the fabricated PLLA, Gel and PLLA/Gel NFs, imaged by SEM, is shown in Fig. 1. Electrospun fibers are characterized by a cylindrical shape, with a highly uniform, smooth and beadless surface. The ES parameters (solution concentration, voltage and injection flow) are optimized in order to achieve fiber diameters ranging from 250 to 550 nm, comparable with the size of native ECM fibrils.[35] We successfully electrospin blends of PLLA and Gel polymers from HFIP solutions. HFIP is capable of dissolving both the synthetic and the natural polymer used in our work. Though some reports highlight protein denaturation following collagen electrospinning from HFIP solutions,[36] this solvent is very effective and suitable to produce Gel-based fibers, since gelatin is already marked by destructed α-chains, disrupted triple-helical and fibrillar structure, and already lacks internal structure or configurational order.[37] For all samples, the diameter distribution is well described by a Gaussian curve, peaked at (420 ± 84) nm, (408 ± 64) nm, and (390 ± 50) nm for PLLA (Fig. 1a and b), Gel (Fig. 1c and d) and PLLA/Gel (Fig. 1e and f), respectively. In addition, more than 70% of the NFs have a diameter in the range 300–450 nm. As-spun Gel NFs are highly water-soluble and brittle, and consequently ineffective for most biomedical applications,[30] hence we crosslink Gel and PLLA/Gel scaffolds by ethyl-dimethylaminopropylcarbodiimide hydrochloride/*N*-hydroxysuccinimide (EDC/NHS) chemistry.[30,38] EDC is less cytotoxic, however it facilitates the formation of amide bonds between carboxylic and amino groups of Gel molecules, without becoming part of the resultant linkage and without leaving residues on the crosslinked scaffolds. EDC is used in the presence of NHS, which helps to prevent the formation of side products and increases the reaction rate.[39] After crosslinking, we check by SEM whether the NFs preserve their initial size (data not shown). In addition, for all the scaffolds we evaluate the degradation profile, which is a key feature of a tissue engineered construct, because the formation of a new tissue is also related to the degradation of the underlying biomaterial. The degradation of PLLA occurs very slowly, with a weight loss of only 5% after 30 days (Fig. 2), in agreement with previous reports and leading to the conclusion that PLLA needs a quite long period (≥24 months) to completely degrade.[40] In contrast, a more significant weight loss is observed for both Gel and PLLA/Gel scaffolds, showing a slight weight loss after 1 day, that reaches 6% (25%) and 10% (14%) after 15 (30) days for Gel and PLLA/Gel, respectively. These results confirm the EDC/NHS induced crosslinking of the Gel-based NFs, which would become more water-resistant but also able to gradually dissolve after the implantation of the scaffolds. In order to provide a vascularized construct, such gradual dissolution of Gel and PLLA/Gel scaffolds is indeed especially beneficial, since the dissolved gelatin gradually creates space for HMEC-1 penetration and migration into inner layers of the scaffolds.[41] The FTIR spectroscopy of PLLA nanofibrous scaffolds evidences the characteristic absorption band [indicated by (1) in Fig. 3], originating from C=O stretching vibrations in the carbonyl group at 1758 cm^{-1},[42] and two bands at 1185 cm^{-1} (2) and 1088 cm^{-1} (3), attributable to backbone ester groups.[43,44] Gel NFs present two bands corresponding to the amide I and amide II at 1629 cm^{-1} (4) and 1538 cm^{-1} (5),[45] predominantly arising from C=O stretching vibrations, and amide N–H bending and C–N stretching vibrations, respectively.[43] In addition, the Gel spectrum presents a broad band (6) due to the overlapping of N–H and O–H stretching vibrations (3300–3600 cm^{-1}).[45,46] The PLLA/Gel NFs show only the same characteristic bands of each constituent polymer, without the appearance of new absorption bands as a possible consequence of reactions in the blend systems, and –OH and $–NH_2$ groups available as binding sites for serum proteins and for then promoting endothelial cell adhesion.[47,48] Overall, the chemistry of blend nanofibrous scaffolds is therefore largely derived from that of the constituent materials, which could induce one to expect surface properties and wetting behavior of blend samples based on those of individual pristine polymers. However, as we report in the following, the wettability of blend nanofibrous scaffolds is not intermediate between those of nanofibrous scaffolds made by single electrospun polymers, a feature which will be shown to strongly affect EC adhesion and viability and which can be useful for designing scaffold architectures with improved properties.

The elastic modulus (Fig. 4a), strain (Fig. 4b), and tensile strength (Fig. 4c) are determined from the stress–strain curves of PLLA, cross-linked Gel and PLLA/Gel NF dry scaffolds. As expected, the mechanical properties of PLLA/Gel are intermediate between the pure Gel (cross-linked) and PLLA. For instance, the elastic modulus of pure PLLA, Gel, and PLLA/Gel NFs is of (200 ± 18) MPa, (368 ± 35) MPa, and (233 ± 34) MPa, respectively. Correspondingly, PLLA NFs present the highest elongation at break (60 ± 9)% [Gel NFs: (13 ± 5)%, PLLA/Gel NFs: (38 ± 9)%] and the lower tensile strength, (6 ± 1) MPa [Gel NFs: (12 ± 2) MPa, PLLA/Gel NFs: (10 ± 1) MPa]. The tensile strength and the elastic modulus of the Gel and PLLA/Gel scaffolds are enhanced with respect to PLLA, as a consequence

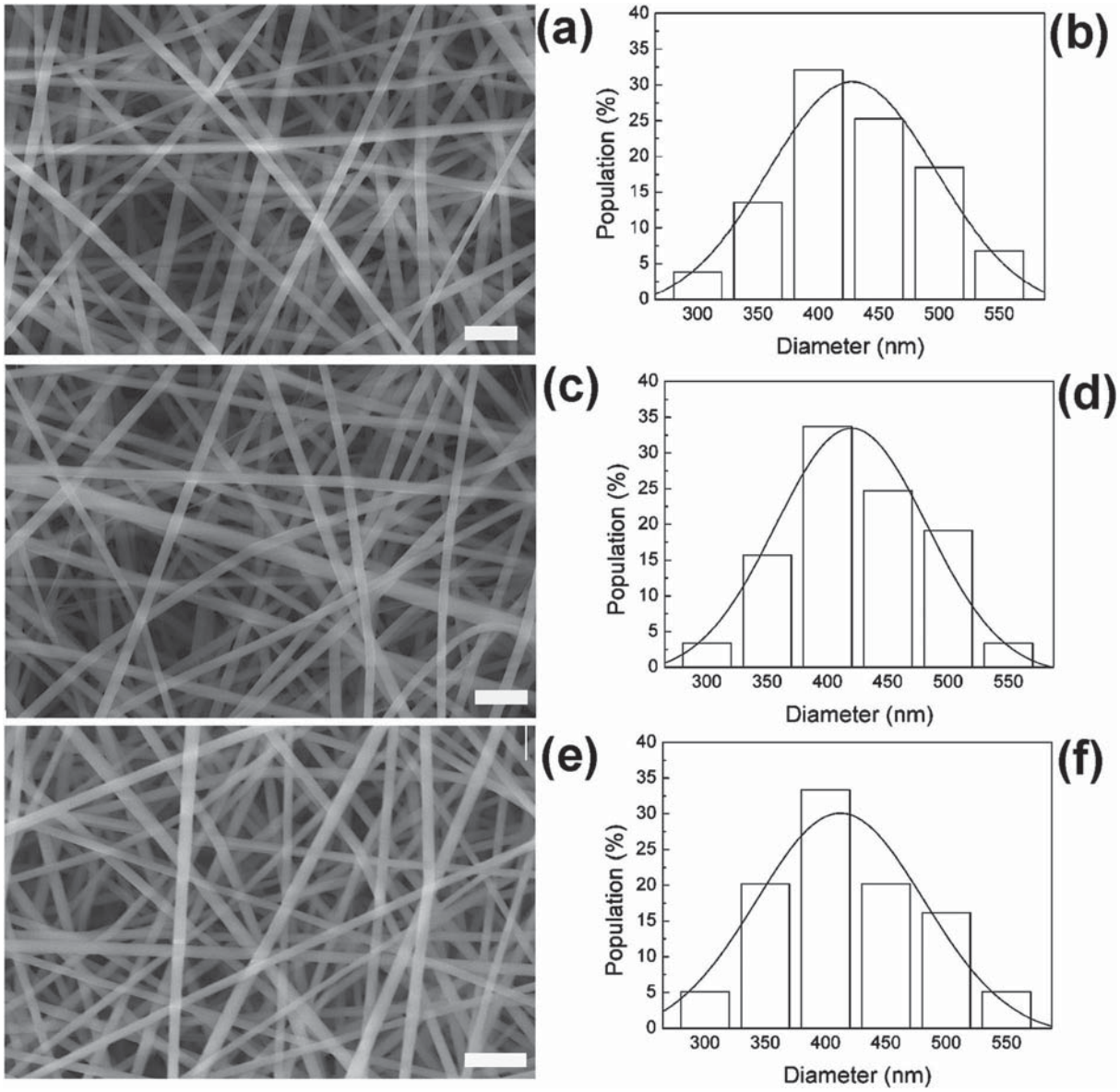

Fig. 1 SEM micrographs of PLLA (a), Gel (c) and PLLA/Gel (e) nanofibers (scale bar: 2 μm), and corresponding distributions of fiber diameters for PLLA (b), Gel (d), and PLLA/Gel (f). The superimposed lines are the best fits by Gaussian curves.

of crosslinking.[30,49] The Gel NFs analyzed before the EDC/NHS-induced crosslinking exhibit an elastic modulus of (91 ± 9) MPa, and a tensile strength of 2.4 ± 0.8 MPa, in agreement with previous studies[50] thus providing electrospun scaffolds that combine biocompatibility with a good mechanical support capacity. As mentioned above, water wettability is also fundamental to promote cell colonization of the biocompatible surface. The pristine PLLA scaffold shows a hydrophobic behaviour with a static WCA (θ) of 118° ± 7° (Fig. 5a–e), whereas the wettability is strongly enhanced by plasma oxygen, leading to a WCA of 40° ± 5° analogous to values measured for Gel (45° ± 5°). A noteworthy finding is that the PLLA/Gel blend turns out to be more hydrophilic ($\theta = 38° \pm 4°$) than both its single components, which is a promising indication in view of promoting cell adhesion, spreading and growth.[11,51] A similar behaviour is also observed for blend films ($\theta = 35° \pm 4°$, in the case of a PLLA/Gel blend with 50 : 50 relative weights, Fig. 5f–i). This finding, analogous to previous results obtained in blend polymer films,[52,53] is in striking contrast with most frequently used modelling approaches describing the contact angle of chemically heterogeneous surfaces as simply given by a linear combination of values obtained on surfaces made by the individual component species (A and B), *i.e.* $\cos\theta = (\cos\theta_B - \cos\theta_A)\,c + \cos\theta_A$, where c is the relative B/A concentration in the blend ($0 \le c \le 1$ with $c = 0$ and $c = 1$ for the pure A and the pure B material, respectively).[54]

To better rationalize our results, the wetting behaviour is measured for six species of NFs and films prepared with different PLLA and Gel ratios. As shown in Fig. 6a, the composition significantly affects water wettability. Blends with Gel content about 10% in weight become more hydrophilic, however the contact angle decreases upon increasing the Gel

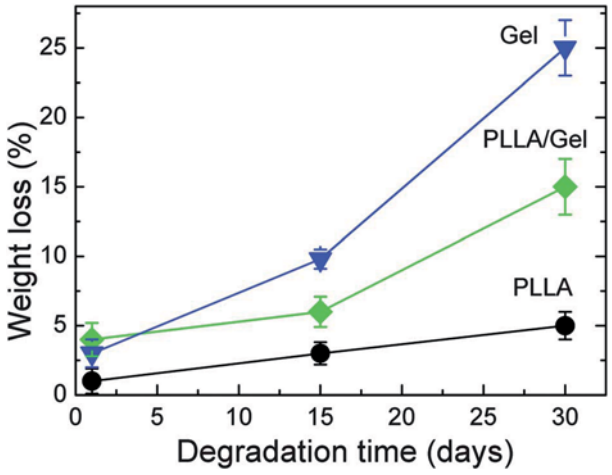

Fig. 2 Degradation behavior of the electrospun nanofibrous supports, described by percentage weight loss *vs.* degradation time for PLLA (circles), Gel (triangles) and PLLA/Gel (diamonds) NFs.

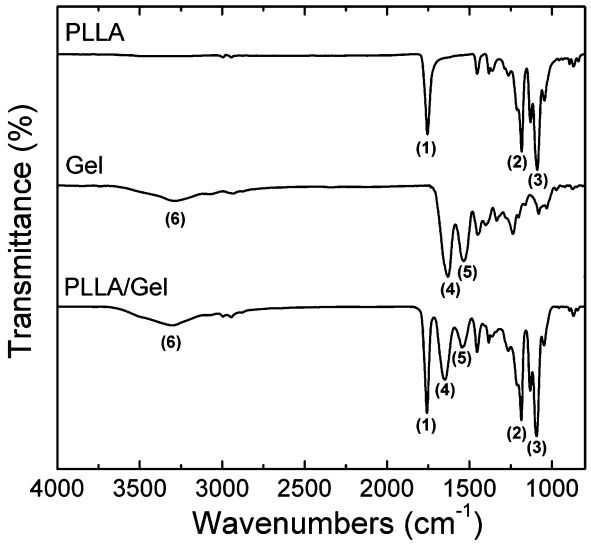

Fig. 3 FTIR spectra of PLLA, Gel and PLLA/Gel NFs (from top to bottom). Relevant transitions: (1) 1758 cm^{-1}, (2) 1185 cm^{-1} and (3) 1088 cm^{-1} are typical bands of PLLA, whereas (4) 1629 cm^{-1}, (5) 1538 cm^{-1} and (6) 3330–3600 cm^{-1} relate to the Gel component, respectively.

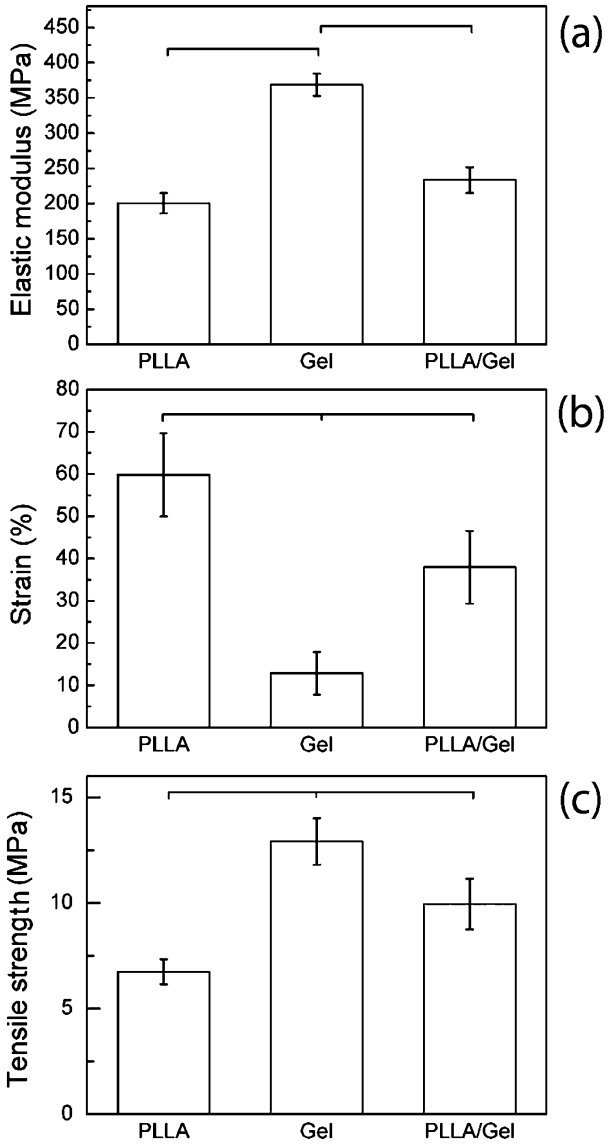

Fig. 4 Elastic modulus (a), strain (b), and tensile strength (c) of the produced NFs. Results are expressed as (mean ± standard deviation). Bars show statistically significant differences ($P < 0.05$).

content is not monotonic. Instead, the enhanced hydrophilicity is especially distinctive of PLLA/Gel NFs with 50 : 50 relative weights. In view of correlating the observed enhanced wettability properties with HMEC-1 adhesion and proliferation, we schematize the nanofibrous surface topography and chemical heterogeneity correlating the resulting properties of the blend-based scaffold with those of the constituent polymeric materials in a different way. As demonstrated in a pioneering study by Tuteja *et al.*,[55] for surfaces exhibiting complex, possibly multi-scale texturing, as in the case of a non-woven nanofiber, a third parameter, namely the local surface curvature in correspondence with the individual nanostructures, has to be added to roughness and surface energy in order to draw a reliable description of the wettability behaviour. Indeed, nanofibrous scaffolds deposited on an underneath substrate exhibit natural re-entrant curvatures, whose effect can be described by simultaneously accounting for the roughness parameter (*i.e.* $r > 1$ in the well-known Wenzel model, indicating the ratio of the overall area of the wetted structured surface to the apparent area)[56] and the low surface-fraction of the wetted surface projected on the horizontal plane (*i.e.* $\Phi < 1$ in the Cassie–Baxter model).[57] Consequently, the behaviour of the contact angle of the nanofibrous polymer surfaces can be explained by considering drops in an intermediate state, with the liquid sitting partially on air[58] as schematized in Fig. 6b. This is described by a modified Cassie–Baxter model,[59] where the corresponding change in surface free energy, ΔF, upon displacing the surface of the liquid–gas interface by an amount, ΔA, is given by:

$$\Delta F = (\gamma_{SL} - \gamma_{SV})\, r\Phi\Delta A + \gamma_{LV}\,(1 - \Phi)\,\Delta A + \gamma_{LV}\cos\theta\Delta A. \quad (1)$$

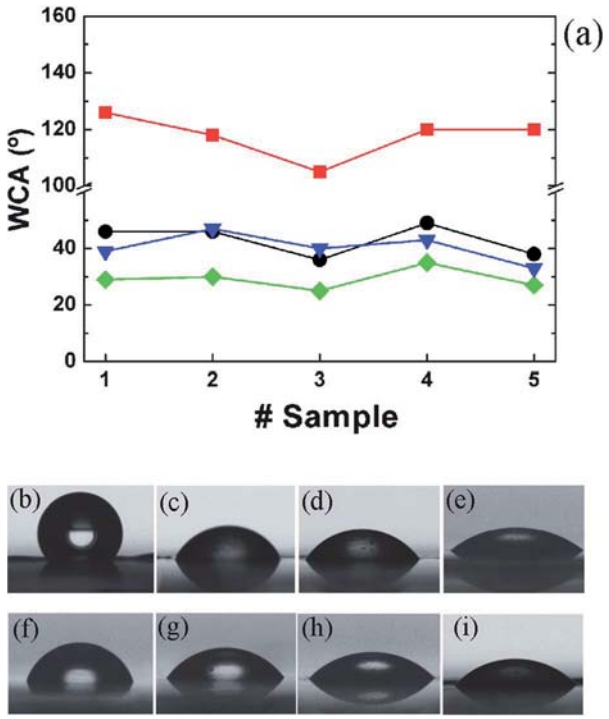

Fig. 5 (a) WCA values for different nanofibrous scaffolds (# = 1–5) of as-spun (square) and plasma-treated PLLA (circles), Gel (triangles), and PLLA/Gel (diamonds) NFs. Lines are guides for the eyes. Middle panels: optical micrographs of water droplets onto as-spun (b) and plasma treated (c) nanofibrous PLLA (b), Gel (d) and PLLA/Gel (e) surfaces. Bottom panels (f–i) show the corresponding photographs on reference film samples.

In the previous expression γ_{SL}, γ_{SV}, and γ_{LV} are the solid–liquid, solid–vapour, and liquid–vapour interfacial tensions, respectively and θ indicates the contact angle on the textured surface. According to eqn (1), the equilibrium contact angle of the nanofibrous scaffold for each electrospun material or blend can be related to that of the corresponding spin-cast samples, θ_0, and to the scaffold surface topology by the following expression:

$$\cos\theta = r\Phi\cos\theta_0 - (1 - \Phi). \quad (2)$$

Applying this model to our investigated systems (PLLA, Gel, and different PLLA/Gel blends) we find that it describes well the contact angle behaviour of all the nanofibrous mats. Schematizing fibers as cylindrical bodies of a circular cross-section with radius (R in Fig. 6b) as measured by SEM, and considering the geometrical dependency of r and Φ on the depth of the wetted fraction [$h = R(1 - \cos\alpha)$ in Fig. 6b] and the surface density of fibers in the top layer of the mat, we obtain the geometrical parameter, α and consequently r and Φ for each scaffold material and blend (bottom panel in Fig. 6a). We find that all the fibrous systems are well described by $1.1 < r < 1.6$ and $0.4 \leq \Phi \leq 0.8$. Both the model roughness parameter and the surface fraction of the wetted surface increase upon increasing the PLLA weight content in the blend, with the highest average values achieved at the 50 : 50 nanofibrous scaffold, resulting in an estimated depth of the wetted fraction of 180 nm.

Given the analogous ensemble nanofibrous topology (*i.e.*, the similar non-woven structure, fiber average diameter and size distribution) to better investigate surface morphology and its relation with wettability properties we also investigate films of PLLA, PLLA/Gel (50 : 50) and Gel by AFM. Fig. 7 shows typical AFM micrographs of the three films and the corresponding photographs of water drops residing on their surfaces. Homopolymer films exhibit very different morphologies, with PLLA being characterized by a micro-patterned, honeycomb-like topography and a root mean square roughness (r_q) of 88 nm, while Gel films exhibit a very smooth surface ($r_q \sim 1$ nm). A co-continuous phase separation, with pores on the sub-micrometre length-scale and an overall roughness, $r_q \sim 22$ nm, can be

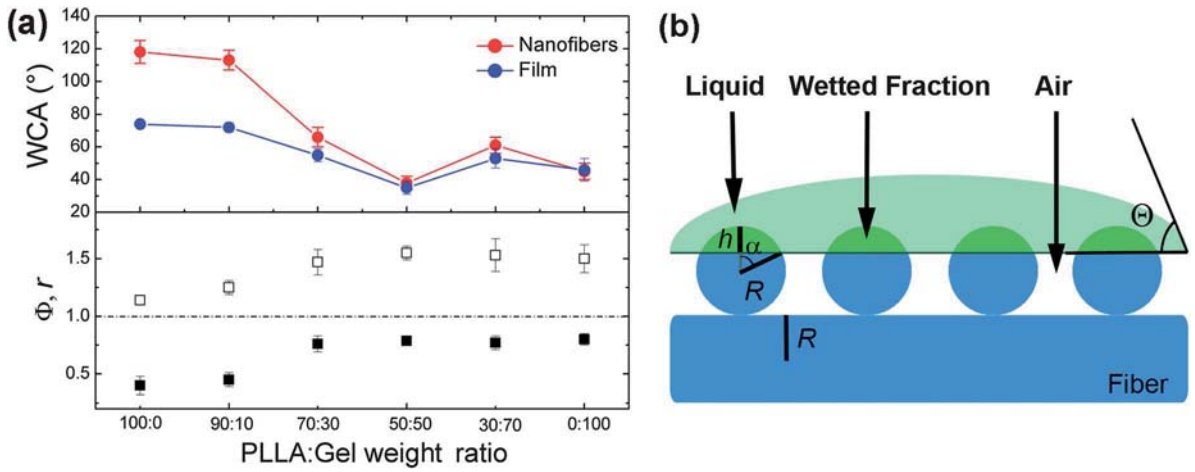

Fig. 6 (a) Top panel: WCA values of PLLA/Gel NFs (red dots) and films (blue dots) containing PLLA and Gel at different weight ratios. Lines are guides for the eyes. Bottom panel: Corresponding Φ (full squares) and r (empty squares) parameters according to the modified Cassie–Baxter state (eqn (2)). The horizontal dash-dotted line indicates unity. (b) Schematic of the partial penetration of the liquid on re-entrant nanofibrous topography and of the modified Cassie–Baxter state. h indicates the liquid penetration depth within the fibrous layer, defined as $h = R(1 - \cos\alpha)$ where R is the fiber radius and α is the geometrical parameter identifying the partial liquid penetration.

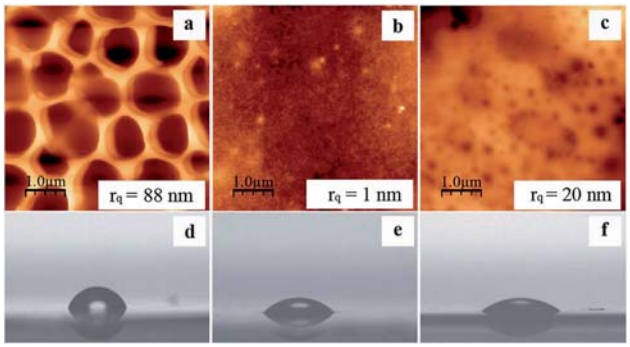

Fig. 7 Atomic Force Microscopy micrographs of (a) PLLA, (b) Gel and (c) PLLA/Gel (50 : 50) films. Vertical scale bars are 480, 11 and 165 nm, respectively. r_q: corresponding measured root mean square roughness. Photographs of water drops (≈ 2 μL) on the surface of (d) PLLA, (e) Gel and (f) PLLA/Gel (50 : 50) films.

instead appreciated in the blend. In agreement with previous reports, sub-μm morphologies which enhance the hydrophilic behaviour of the blend through the partial penetration of the liquid within the recessed features of the surface[59,60] and the favourable reorientation of hydrophilic moieties towards the scaffold surface which may occur upon blending[60] may account for the enhanced wettability of the blend in both films and fibers. Once the enhanced wettability properties have been assessed, we proceed to investigate how the 50 : 50 blend nanofibrous scaffolds outperform those based on pristine polymer NFs in terms of microvascular EC proliferation and viability.

Cell proliferation and CD31 expression

HMEC-1 is the first immortalized human microvascular endothelial cell line that retains the morphologic, phenotypic, and functional characteristics of normal human microvascular ECs, showing no sign of senescence even after 95 passages (normal microvascular ECs undergo senescence at passages 8–10).[33] We exploit for the first time HMEC-1 cells for testing the ability of electrospun scaffolds to favor endothelial cell adhesion, proliferation and functionality. The viability, proliferation, and mitochondrial activity of HMEC-1 cells are evaluated after 2, 4 and 8 days on nanofibrous scaffolds (Fig. 8a). MTS assays highlight the absence of cytotoxicity in our scaffolds for HMEC-1. These results well agree with those reported from Yang *et al.*, showing that cells grown with potential traces of HFIP stained with a deadlive kit show negligible cell death, and that cells largely remain viable.[61] This is further supported by proliferation experiments, evidencing that different NF scaffolds are significant to cell proliferation during culture (Fig. 8a).

In particular, we find that, while after 2 days the number of cells on the different supports is roughly comparable (in the range of 3.1–3.5 × 10^4 cells), after 4 days the scaffolds containing Gel exhibit an enhanced cell proliferation compared to pure PLLA NFs, and this trend is more evident after 8 days (at the last time point, PLLA NFs: 5 × 10^4 cells, Gel NFs: 6 × 10^4 cells, PLLA/Gel NFs: 7 × 10^4 cells). In particular, after 8 days of HMEC-1 culture the number of metabolically active cells on PLLA, Gel and PLLA/Gel scaffolds is about 1.6, 1.9, and 2.3 times higher than those initially seeded, respectively, highlighting the best proliferation on the blend polymer system. For the sake of

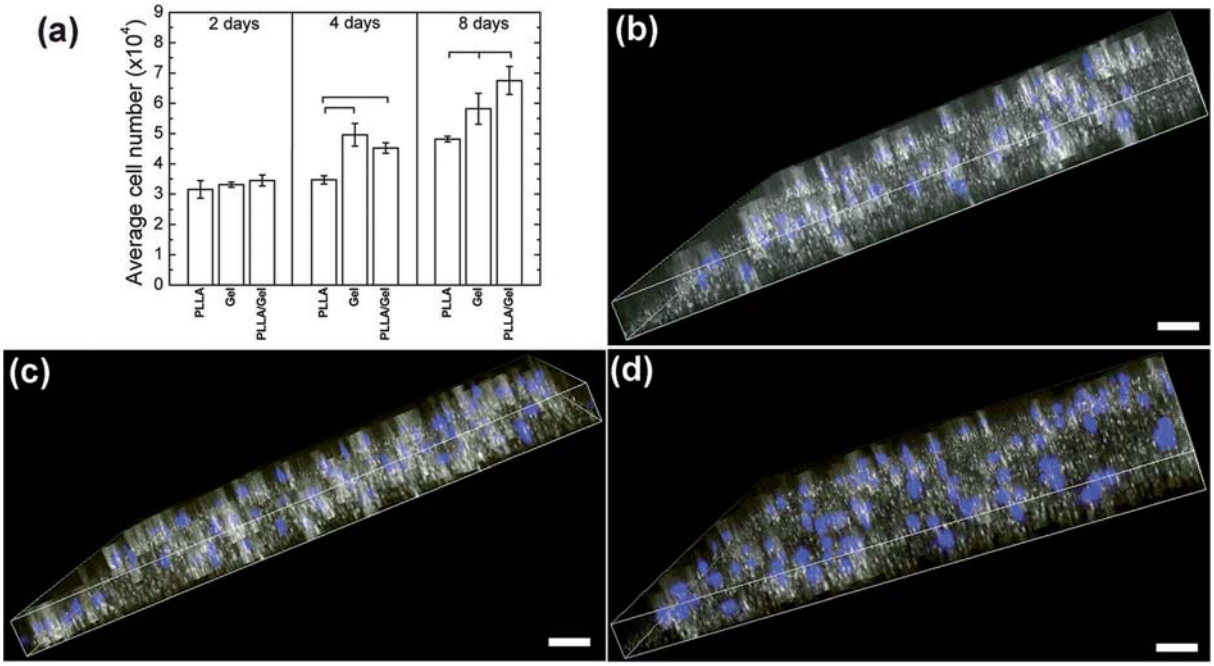

Fig. 8 (a) MTS assay describing HMEC-1 proliferation on the electrospun scaffolds after various incubation periods (2, 4, and 8 days). Results are expressed as (mean ± standard deviation). Bars show statistically significant differences ($P < 0.05$) (b–d). Three dimensional occupation of DNA stained (DAPI, blue color) HMEC-1 cells within the electrospun (b) PLLA, (c) Gel and (d) PLLA/Gel scaffolds. Scale bars = 80 μm.

comparison, control cultures on polystyrene allow reaching an analogous number of active cells (around 2.3 times higher than those initially seeded). These results evidence that nanofibrous substrates, and in particular 50 : 50 PLLA/Gel NFs, allow reaching proliferation rates fully matching optimal growth on tissue culture-treated polystyrene dishes. Electrospun supports blending synthetic and natural polymers are therefore an optimal environment for HMEC-1 growth. Though it is not surprising that a blend containing both PLLA and Gel has a better cytocompatibility than pure PLLA scaffolds, the higher cell proliferation rate observed on PLLA/Gel with respect to Gel NFs is a significant result which may be strictly related to the enhanced wettability properties observed in the blend. Three-dimensional confocal microscopic studies are also performed, not only to directly visualize cell proliferation, but, more interestingly, to disclose the penetration of HMEC-1 cells into inner layers and interstices, deep below the superficial layers of fibers of the scaffolds. A substantial penetration of cells into the nanofibrous structure is observed for all the scaffold formulations (Fig. 8b–d), which is a remarkable outcome in view of developing tissue engineered scaffolds supporting endothelial cellular infiltration and ingrowth.[62] The initial phase of cell–scaffold communication is represented by cell adhesion which in turn promotes a series of different cell responses inclusive of spreading, proliferation and differentiation. Upon cell attachment and spreading[63] on the scaffolds, we study the cytoskeleton organization of HMEC-1 cells by staining actin filaments with Phalloidin Fluorescein Isothiocyanate Labeled (phalloidin-FITC), and nuclei with DAPI (Fig. 9). The results confirm that cells retain the typical adherent and spreading morphology, showing well-stretched actin bundles without appreciable differences on the different scaffolds (Fig. 9a, c and e). However, when analyzing the phenotypic properties as well as the functional development of ECs through the expression of a typical endothelial cell marker, the CD31 protein, we find a better expression and adequate inter-endothelial contacts between adjacent cells especially on PLLA/Gel NFs (Fig. 9b, d and f). In fact, it is well established that the scaffolds could affect the synthesis of molecules for homotypic adhesion (CD31, VE-cadherin) or of integrin for the adhesion onto the substrate,[64] and CD31 is involved in endothelial cell–cell adhesion and plays an important role in ensuring the endothelial barrier integrity.[65] This immunocytochemical analysis, besides evidencing the highest cell density on PLLA/Gel in agreement with results from proliferation tests, highlights therefore a better functionality as induced by the electrospun PLLA/Gel scaffolds. In a very few reports, blend polymer NFs are demonstrated to induce an improved response with respect to purely synthetic samples in a variety of different cellular species.[20,29] For instance, PCL/Gel NFs with a relative concentration of 70 : 30 have been studied as scaffolds for the growth of neural stem cells, promoting and directing the neurite outgrowth.[20] Here, the blend NFs, combining the mechanical properties of the synthetic polymer and the Gel biocompatibility, result in engineered supports with enhanced wettability, that triggers the most favorable EC adhesion processes and supports the rapid growth and formation of inter endothelial contacts. Enhanced wetting properties

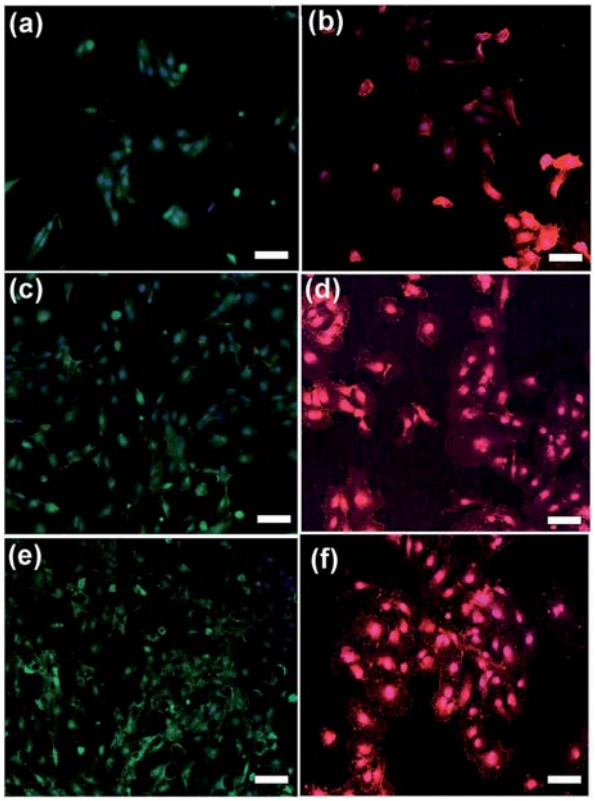

Fig. 9 Cytoskeleton arrangement and CD31 immunocytochemistry of HMEC-1 cells grown on PLLA (a and b), Gel (c and d) and PLLA/Gel (e and f) NFs (scale bars: 100 μm). (a, c and e) Merged confocal images of stained DNA (DAPI, blue color), actin (FITC-phalloidin, green color). (b, d and f) Merged confocal images of stained CD31 (Alexa fluor 555-red) and DNA-(DAPI blue) stained cells.

may impact cell adhesion and viability through several mechanisms. In particular, the adsorption of serum proteins is demonstrated to play a key role for the cell proliferation, adhering unspecifically on nanofibrous scaffolds with rates that can be significantly affected by the degree of hydrophilicity.[11] Overall, highly wettable blend NFs are of particular interest in view of achieving pre-vascularized scaffolds for functional tissue engineered implants, with ECs easily available in perspective to form an effectively functioning vasculature after implantation.

Conclusions

In this work blend polymer nanofibrous scaffolds are produced by ES with the aim of studying their ability to favour EC adhesion, proliferation and functionality. We investigate for the first time the behaviour of HMEC-1 cells on NFs and focus on the analysis of the wettability properties of blend nanofibrous scaffolds, which exhibit the best performances in terms of cell proliferation and viability. Our results demonstrate that the realized bioartificial tissues possess favourable morphological, chemical, degradation and mechanical properties, and they are able to support EC spreading and growth. In particular, we find higher proliferation rates and improved endothelial functionality for ECs on blend polymer scaffolds.

We anticipate that the production of electrospun scaffolds by blending synthetic and bio polymers with enhanced wettability is a promising strategy to dispose of supports for regeneration of big tissues that have relevant vascularization issues and requirements.

Acknowledgements

The authors acknowledge the support of the Italian Ministry of University and Research through the FIRB Contract RBNE08BNL7 (MERIT Program) and Dr. Carola La Tegola for the technical support during mechanical analysis.

Notes and references

1 A. Atala, *Curr. Opin. Biotechnol.*, 2009, **20**, 575–592.
2 R. Langer and D. A. Tirrell, *Nature*, 2004, **428**, 487–492.
3 V. P. Shastri, *Adv. Mater.*, 2009, **21**, 3246–3254.
4 J. Leor, Y. Amsalem and S. Cohen, *Pharmacol. Ther.*, 2005, **105**, 151–163.
5 J. Rouwkema, N. C. Rivron and C. A. van Blitterswijk, *Trends Biotechnol.*, 2008, **26**, 434–441.
6 R. K. Jain, P. Au, J. Tam, D. G. Duda and D. Fukumura, *Nat. Biotechnol.*, 2005, **23**, 821–823.
7 S. Levenberg, J. Rouwkema, M. Macdonald, E. S. Garfein, D. S. Kohane, D. C. Darland, R. Marini, C. A. van Blitterswijk, R. C. Mulligan, P. A. D'Amore and R. Langer, *Nat. Biotechnol.*, 2005, **23**, 879–884.
8 R. E. Unger, S. Ghanaati, C. Orth, A. Sartoris, M. Barbeck, S. Halstenberg, A. Motta, C. Migliaresi and C. J. Kirkpatrick, *Biomaterials*, 2010, **31**, 6959–6967.
9 P. L. Tremblay, V. Hudon, F. Berthod, L. Germain and F. A. Auger, *Am. J. Transplant.*, 2005, **5**, 1002–1010.
10 S. H. Lim and H. Q. Mao, *Adv. Drug Delivery Rev.*, 2009, **5**, 1084–1096.
11 A. Polini, S. Pagliara, R. Stabile, G. S. Netti, L. Roca, C. Prattichizzo, L. Gesualdo, R. Cingolani and D. Pisignano, *Soft Matter*, 2010, **6**, 1668–1674.
12 A. Polini, D. Pisignano, M. Parodi, R. Quarto and S. Scaglione, *PLoS One*, 2011, **6**, e26211.
13 X. M. Mo, C. Y. Xu, M. Kotaki and S. Ramakrishna, *Biomaterials*, 2004, **25**, 1883–1890.
14 C. A. Bashur, L. A. Dahlgren and A. S. Goldstein, *Biomaterials*, 2006, **27**, 5681–5688.
15 L. Ricotti, A. Polini, G. G. Genchi, G. Ciofani, D. Iandolo, H. Vazão, V. Mattoli, L. Ferreira, A. Menciassi and D. Pisignano, *Biomed. Mater.*, 2012, **7**, 035010.
16 M. Whited, J. R. Whitney, M. C. Hofmann, Y. Xu and M. N. Rylander, *Biomaterials*, 2011, **32**, 2294–2304.
17 J. Stitzel, L. Liu, S. J. Lee, M. Komura, J. Berry, S. Soker, G. Lim, M. Van Dyke, R. Czerw, J. J. Yoo and A. Atala, *Biomaterials*, 2006, **27**, 1088–1094.
18 H. M. Powell and S. T. Boyce, *Tissue Eng., Part A*, 2009, **15**, 2177–2187.
19 N. Bhattarai, D. Edmondson, O. Veiseh, F. A. Matsen and M. Zhang, *Biomaterials*, 2005, **26**, 6176–6184.
20 L. Ghasemi-Mobarakeh, M. P. Prabhakaran, M. Morshed, M. H. Nasr-Esfahani and S. Ramakrishna, *Biomaterials*, 2008, **29**, 4532–4539.
21 J. Nanobashvili, C. Neumayer, A. Fugl, E. Sporn, P. Polterauer and I. Huk, *Eur. Surg.*, 2003, **35**, 214–218.
22 Y. Xu, R. A. Swerlick, N. Sepp, D. Bosse, E. W. Ades and T. J. Lawley, *J. Invest. Dermatol.*, 1994, **102**, 833–837.
23 E. Cenni, F. Perut and N. Baldini, *Acta Pharmacol. Sin.*, 2011, **32**, 21–30.
24 F. Yang, R. Murugan, S. Wang and S. Ramakrishna, *Biomaterials*, 2005, **26**, 2603–2610.
25 H. Zhu, J. Ji, M. A. Barbosa and J. Shen, *J. Biomed. Mater. Res., Part B*, 2004, **71**, 159–165.
26 L. Zhang and T. J. Webster, *Nano Today*, 2009, **4**, 66–80.
27 E. Seyedjafari, M. Soleimani, N. Ghaemi and I. Shabani, *Biomacromolecules*, 2010, **11**, 3118–3125.
28 Y. L. Cui, A. D. Qi, W. G. Liu, X. H. Wang, H. Wang, D. M. Ma and K. D. Yao, *Biomaterials*, 2003, **24**, 3859–3868.
29 H. W. Kim, H. S. Yu and H. H. Lee, *J. Biomed. Mater. Res., Part A*, 2008, **87**, 25–32.
30 Y. Z. Zhang, J. Venugopal, Z.-M. Huang, C. T. Lim and S. Ramakrishna, *Polymer*, 2006, **8**, 2911–2917.
31 S. Y. Gu, Z. M. Wang, J. Ren and C. Y. Zhang, *Mater. Sci. Eng., C*, 2009, **29**, 1822–1828.
32 M. P. Prabhakaran, J. Venugopal and S. Ramakrishna, *Acta Biomater.*, 2009, **5**, 2884–2893.
33 E. W. Ades, F. J. Candal, R. A. Swerlick, V. G. George, S. Summers, D. C. Bosse and T. J. Lawley, *J. Invest. Dermatol.*, 1992, **99**, 683–690.
34 S. E. Kim, D. N. Heo, J. B. Lee, J. R. Kim, S. H. Park, S. H. Jeon and I. K. Kwon, *Biomed. Mater.*, 2009, **4**, 044106.
35 C. P. Barnes, S. A. Sell, E. D. Boland, D. G. Simpson and G. L. Bowlin, *Adv. Drug Delivery Rev.*, 2007, **59**, 1413–1433.
36 L. Yang, C. C. F. Fitie, K. O. van der Werf, M. L. Bennink, P. J. Dijkstra and J. Feijen, *Biomaterials*, 2008, **29**, 955–962.
37 A. Veis, J. Anesey and J. Cohen, *Arch. Biochem. Biophys.*, 1961, **94**, 20–31.
38 S. Xu, J. Li, A. He, W. Liu, X. Jiang and J. Zheng, *Polymer*, 2009, **50**, 3762–3769.
39 S. Torres-Giner, J. V. Gimeno-Alcañiz, M. J. Ocio and J. M. Lagaron, *ACS Appl. Mater. Interfaces*, 2009, **1**, 218–223.
40 K. Rezwan, Q. Z. Chen, J. J. Blaker and A. R. Boccaccini, *Biomaterials*, 2006, **27**, 3413–3435.
41 Y. Zhang, H. Ouyang, C. T. Lim, S. Ramakrishna and Z. M. Huang, *J. Biomed. Mater. Res., Part B*, 2005, **72**, 156–165.
42 O. N. Tretinnikov, K. Kato and H. Iwata, *Langmuir*, 2004, **20**, 6748–6753.
43 A. Sionkowska, M. Wisniewski, J. Skopinska, C. J. Kennedy and T. J. Wess, *Biomaterials*, 2004, **25**, 795–801.
44 S. Inkinen, M. Hakkarainen, A. C. Albertsson and A. Södergård, *Biomacromolecules*, 2011, **14**, 523–532.
45 J. H. Ko, H. Y. Yin, J. An, D. J. Chung, J. H. Kim, S. B. Lee and D. G. Pyun, *Macromol. Res.*, 2010, **18**, 137–143.
46 J. P. Chen and C. H. Su, *Acta Biomater.*, 2011, **7**, 234–243.
47 K. J. An, H. Liu, S. Guo, D. N. T. Kumar and Q. Wang, *Int. J. Biol. Macromol.*, 2010, **47**, 380–388.

48 J. G. Steele, G. Johnson, C. McFarland, B. A. Dalton, T. R. Gengenbach and R. C. Chatelier, *J. Biomater. Sci., Polym. Ed.*, 1994, **6**, 511–532.
49 S. Zhang, Y. Huang, X. Yang, F. Mei, Q. Ma, G. Chen, S. Ryu and X. Deng, *J. Biomed. Mater. Res., Part A*, 2009, **90**, 671–679.
50 Z.-M. Huang, Y. Z. Zhang, S. Ramakrishna and C. T. Limb, *Polymer*, 2004, **45**, 5361–5368.
51 Z. X. Meng, W. Zhenga, L. Lia and Y. F. Zheng, *Mater. Chem. Phys.*, 2011, **125**, 606–611.
52 I. O. Ucar, M. D. Doganci, C. E. Cansoy, H. Y. Erbil, I. Avramova and S. Suzer, *Appl. Surf. Sci.*, 2011, **257**, 9587–9594.
53 X. Zhao, W. Liu and K. Yao, *J. Appl. Polym. Sci.*, 2006, **101**, 269–276.
54 K. Seki and M. Tachiya, *J. Phys. Chem. B*, 2004, **108**, 4806–4810.
55 A. Tuteja, W. Choi, M. Ma, J. M. Mabry, S. A. Mazzella, G. C. Rutledge, G. H. McKinley and R. E. Cohen, *Science*, 2007, **318**, 1618–1622.
56 R. N. Wenzel, *Ind. Eng. Chem.*, 1936, **28**, 988–994.
57 A. B. D. Cassie and S. Baxter, *Trans. Faraday Soc.*, 1944, **40**, 546–551.
58 N. J. Shirtcliffe, G. McHale, M. I. Newton and C. C. Perry, *Langmuir*, 2005, **21**, 937–943.
59 L. Persano, P. del Carro and D. Pisignano, *Appl. Phys. Lett.*, 2012, **100**, 151607.
60 X. Yang, Q. Xu, N. Yan, G. Sui, Q. Cai, X. Deng and Y. X. Xua, *Polym. Adv. Technol.*, 2011, **22**, 2222–2230.
61 X. Yang and H. Wang, *Biomaterial scaffold fabrication techniques for potential tissue engineering applications*, ed. D. Eberli, 2010, ISBN: 978-953-307-079-7.
62 M. Skotak, J. Ragusa, D. Gonzalez and A. Subramanian, *Biomed. Mater.*, 2011, **6**, 055012.
63 U. Hersel, C. Dahmen and H. Kessler, *Biomaterials*, 2003, **24**, 4382–4415.
64 I. Amato, G. Ciapetti, S. Pagani, G. Marletta, C. Satriano, N. Baldini and D. Granchi, *Biomaterials*, 2007, **28**, 3668–3678.
65 S. M. Albelda, W. A. Muller, C. A. Buck and P. J. Newman, *J. Cell Biol.*, 1991, **114**, 1059–1068.